Optimizing Planar Source Distributions for Deep Power Deposition in Biological Tissue

Carey M. Rappaport
Center for Electromagnetics Research
235 Forsyth Building
Northeastern University
Boston, MA 02115

Abstract

In non-invasive hyperthermia, penetration depth in high water content biological tissue can be increased up to 3 times using a focused instead of uniform surface electric field distribution. The focusing involves maximizing the field integral at a focal point by solving for the surface phase function which makes the integrand real and positive for all surface points. The resulting non-linear differential equation is solved in using a series approximation. A focused power deposition pattern is presented using this ideal planar distribution which is the theoretical optimum for high resolution hyperthermia cancer treatment.

Introduction: EM Cancer Treatment

Favorable responses to electromagnetic heating of tumors to 42° - 45° C has generated interest in developing antenna applicators to assist in treating cancer in humans [Overgaard, 1972, and Hahn, 1982]. Electromagnetic radiation has advantages over other current forms of treatment since it can be administered non-invasively, without anesthesia, and causes minimal side effects. Hyperthermia also shows promise when used in conjunction with standard treatment modalities, by increasing the absorption and response of chemotherapeutic agents or by attacking radiation resistant cells [Strohbehn, 1984]. It is essential in designing these antennas to find field distributions which maximize the deposited power at the tumor, while keeping healthy intervening tissue from overheating. The "best" focused field pattern is one that has at least as much power at the focal target as on the surface or at any locations of secondary maxima.

The current analysis assumes a simple uniform geometric model of tissue volume with a localized tumor at its center, exposed to radiation from a surrounding antenna aperture. Previous work has optimized the source distributions for spherical and cylindrical geometries [Rappaport, 1987, Pereira, 1991, Jouvie, 1986]. This study will examine maximizing the power at the mid-plane of a planar slab, optimally illuminated from both sides. As

such, it provides a benchmark for possible microwave heating of relatively flat portions of the body: primarily chest and abdomen.

Electrical characteristics of human tissue vary non-linearly with frequency: with conductivity increasing and dielectric constant decreasing as frequency increases. To determine the best power dissipation pattern in a volume of tissue, the frequency must be selected to balance the competing effects of exponential wave decay and geometric focusing. A higher frequency wave has a smaller wavelength (and thus decays more rapidly), but can be focused better than a lower frequency wave. The present synthesis effort concerns power deposited in high water content tissue (HWC): muscle, organs, and blood, which has higher conductivity and dielectric constant, and so is more challenging to focus waves at depth in than low water content tissue (LWC): fat and bone.

It has been determined that for a deep, well-formed focal maximum in uniform HWC tissue, 915 MHz is the best standard frequency of electromagnetic radiation [Rappaport, 1988]. Above 915 MHz, the wavelength is too short to take advantage of lower loss per wavelength and increased constructive interference of HWC tissue; while below 915 MHz, the greater tissue conductivity eliminates a high-resolution, well-defined focal maximum. For uniform heating, lower frequencies are better, but to target a localized tumor and minimize heating of the surrounding healthy tissue, frequencies above 500 MHz are necessary. The dielectric constant and conductivity of HWC tissue at 915 MHz are about $\epsilon' = 51$ and $\sigma = 1.28$ S/m [Johnson, 1972].

Optimization Procedure

The method used for deriving the best power pattern in a planar slab involves integrating the surface field distribution. Although the electric field and deposited power can be increased at a focal target in lossy tissue by specifying a conjugate phase distribution on a single planar source irradiating a half-space, it is not possible to raise the power levels at depth to that of the surface [Loane, 1986, Gee, 1984]. To deposit as much heat in the center of a slab model of HWC tissue as on its surface requires balanced excitation from both sides. The maximum thickness of the tissue slab is determined by this focal point global maximum condition, and is a function of frequency and source distribution. It is the point of this study to find this maximum slab thickness.

The standard focusing practice of specifying a conjugate (or time-reversed) source phase distribution maximizes the focal field in free space or lossless media. However, in dissipative media, an additional correction phase function is required to ensure all points of the aperture constructively contribute to the field at the focus. It should also be noted that if the medium is lossy, an infinite, uniform amplitude aperture does not produce infinite field intensity at the focal point.

By first assuming the source fields on opposing source planes have uniform amplitude, the synthesis problem reduces to finding the best phase distribution. The phase function is determined so as to make the integrand purely real for the observation field-point at the focus. This ensures that every point of both source planes adds constructively at the focal target. For other points—both in the longitudinal and transverse directions—there will be some measure of destructive interference, which will enhance the relative power at the focus.

The opposing planar sources, shown in Figure 1, have circular symmetry about a focal axis. The observer point is identified by vector $\bar{r}$. When $\bar{r}$ lies along the axis of symmetry at the point $(0,0,z)$, $d/2+z$ is the distance to the source at $z=-d/2$, and $d/2-z$ is the distance to the source at $z=d/2$. The tangential electric field on the source plane is assumed to be y-polarized with unit amplitude, and have both tangential (radial) and longitudinal (axial) real phase and amplitude dependencies expanded about the axial coordinate at each source:

$$\bar{E}_t(\bar{r}) = \hat{y}e^{j\Phi(\rho)+j\Gamma(\rho)(\frac{d}{2}\pm z)+j\Upsilon(\rho)(\frac{d}{2}\pm z)^2}e^{\Xi(\rho)(\frac{d}{2}\pm z)}e^{\Omega(\rho)O((\frac{d}{2}\pm z)^3)} \tag{1}$$

where $\Phi(\rho)$ is the surface phase radial dependence at $z=\mp d/2$, and the choice of sign preceding z is the positive for the source at $z=-d/2$ with wave propagation to the right, and negative for source at $z=d/2$ propagating to the left. Note that for each source at $z=\pm d/2$ there is no amplitude variation as a function of ρ, but the derivative of $\bar{E}_t$ with respect to z at the surface has non-zero amplitude with radial dependence $\Xi(\rho)$. It will be assumed that the amplitude varies exponentially (with linear exponent rather than as e^{az^2}, or higher order). Similarly, the Γ and Υ phase functions are necessary since the normal derivatives have non-zero phase. All phase dependence higher than second order on z are lumped into the last factor of Equation (1).

Inserting this assumed electric field into the circular cylindrical version of the Helmholtz Equation,

$$(\frac{\partial^2}{\partial z^2}+\frac{1}{\rho}\frac{\partial}{\partial\rho}\rho\frac{\partial}{\partial\rho}+k^2)\bar{E}=0, \tag{2}$$

yields one real and one imaginary equation:

$$\Xi^2-\Gamma^2-\Phi'^2+(\frac{d}{2}\pm z)[...]=\alpha^2-\beta^2 \tag{3}$$

and

$$-2\Gamma\Xi+\Phi''+\frac{\Phi'}{\rho}+2\Upsilon+(\frac{d}{2}\pm z)[...]=2\alpha\beta \tag{4}$$

where Ω and the terms involving derivatives of Φ, Γ, Ξ, and Υ multiplying $(\frac{d}{2}\pm z)$ have been suppressed. The wave number is $k=\beta-j\alpha=(\omega/c)\sqrt{\epsilon'-\sigma/\omega\epsilon_0}$ for radian frequency ω and speed of light c.

At each source, separately, $z=\mp d/2$, Equations (3) and (4) reduce to:

$$\beta^2-\alpha^2-(\beta_z^2-\alpha_z^2)-\Phi'^2=0 \tag{5}$$

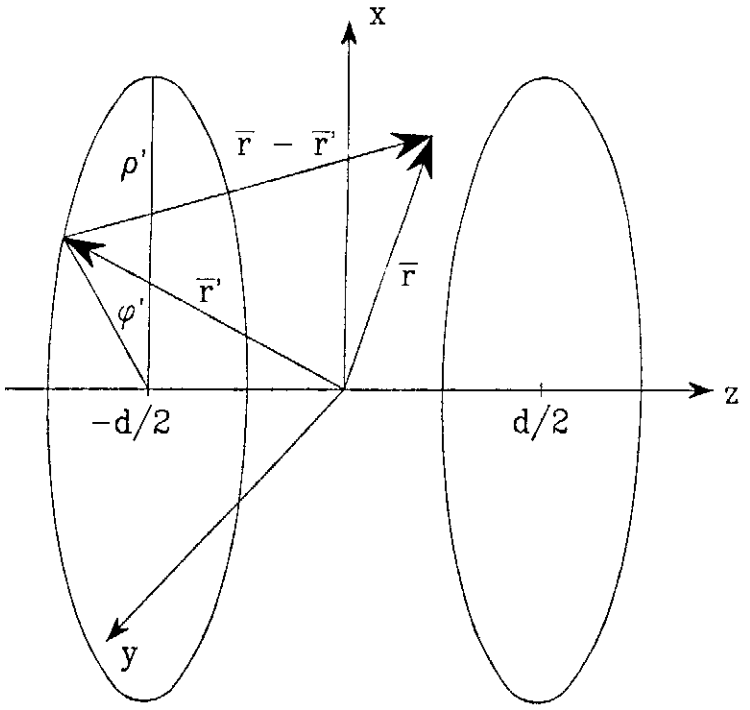

Figure 1: Opposing planar surface source excitation of tissue slab geometry with desired focal target at the origin.

and

$$-2\alpha\beta + 2\alpha_z\beta_z + \Phi'' + \frac{\Phi'}{\rho} + 2\Upsilon = 0 \tag{6}$$

where the natural substitutions, $\Xi(\rho) = -\alpha_z(\rho)$, $\Gamma(\rho) = \beta_z(\rho)$ have been made in analogy with inwardly propagating inclined plane waves.

The derivative of the source phase with respect to radial coordinate, $\Phi'(\rho)$, is thus given in terms of these unknown auxiliary functions representing the normal component of the propagation constant $k_z = \beta_z - j\alpha_z$.

One additional equation is necessary to uniquely specify the phase. This final equation is the focusing condition. The Kirchoff integral equation for electric field caused by unity amplitude surface electric field can be written in terms of the parameters and geometry discussed above as [Kong, 1986],

$$\bar{E}(\bar{r}) = \hat{y}\int_0^{2\pi} d\phi' \int_0^{\infty} \rho' d\rho' \left[j\left(\frac{d/2 \pm z}{R}\beta + \beta_z\right) + \frac{d/2 \pm z}{R}\left(\alpha + \frac{1}{R}\right) + \alpha_z \right] \frac{e^{-j[kR - \Phi(\rho')]}}{4\pi R} \tag{7}$$

where the sources are on the planes at $z = \pm d/2$, and $R = \sqrt{\rho'^2 + (\frac{d}{2} \pm z)^2}$ is the distance from the source point $\bar{r}' = (\rho', \phi', \frac{d}{2})$ to the observation point along the focal axis $\bar{r} =$

$(0,0,z)$. The terms α_z and β_z result from the normal derivatives of the surface electric field. They correspond to the surface magnetic field.

The task is to determine $\Phi(\rho')$ so that the integral of Equation (7) is maximized at the observer focal point, $(\rho, z) = (0,0)$. This condition occurs when the integrand is entirely real and positive for all values of integration arguments ϕ' and ρ'. Writing the entire integrand in magnitude/phase form and setting the phase to zero at the focus, $z = 0$, yields the nonlinear differential equation for Φ:

$$\Phi(\rho') = \beta R_0 - \tan^{-1} \frac{\beta d/2 + \beta_z R_0}{d/2R_0 + \alpha d/2 + \alpha_z R_0} \tag{8}$$

where $R_0 = \sqrt{\rho'^2 + (d/2)^2}$.

Differentiating Equation (8) with respect to ρ' results in:

$$\Phi'(\rho') = \beta \frac{\rho'}{R_0} + \delta(\rho') \tag{9}$$

where the correction phase function $\delta(\rho')$ represents the derivative of the arctangent function. In the subsequent analysis, the primes on the source radius will be suppressed.

In order to solve for $\Phi(\rho)$ using Equations (5), (6) and (9), the values of $\alpha_z(\rho)$ and $\beta_z(\rho)$ must be determined.

If Equation (6) remains finite at $\rho = 0$, the lowest order term of δ must be linear (i.e. $\delta(\rho) = \delta_1 \rho + O(\rho^2)$), and thus $\delta(0) = 0$. Further, since $\delta(\rho)$ is proportional to the derivative of the argument of the arctangent function of Equation (8), which in turn has terms composed of either ρ/R_0, $\partial\alpha_z/\partial\rho$, or $\partial\beta_z/\partial\rho$, then at $\rho = 0$, a possible constraint is:

$$\begin{aligned} \left.\frac{\partial \alpha_z}{\partial \rho}\right|_{\rho=0} &= 0 \\ \left.\frac{\partial \beta_z}{\partial \rho}\right|_{\rho=0} &= 0 \end{aligned} \tag{10}$$

Appealing to Equation (5) and the notion that at $\rho = 0$ the incident wave is entirely normal, it can be safely concluded that $\alpha_z = \alpha + O(\rho^2)$ and $\beta_z = \beta + O(\rho^2)$. Choosing the precise form of α_z and β_z is somewhat arbitrary. As their values increase, the electric field at the focus, given by Equation (7) at $z = 0$ increases, even though the surface electric field stays constant at unity. This is analogous to coupling to a resonator at a point near an electric field null. Since these parameters represent the magnetic field sources, they cannot be selected to be too large at any point on the source surface, since they produce large electric fields one-quarter of a wavelength away. As long as α_z and β_z are bounded to values close to α and β, there will be no non-physical fields resulting from the normal electric field derivatives. Also, since the contributions to the focused field from surface

source points more than several wavelengths away from the focal axis becomes negligible, only the limiting behavior of α_z and β_z near $\rho = 0$ matters.

The phase term $\Upsilon(\rho)$ of Equation (1) represents the second-order normal dependence of the field. As $\rho \to \infty$, $\beta_z \to 0$ (because the wave would be propagating entirely in the radial direction), and the entire z-dependent phase is proportional to $\Upsilon(\rho)z^2$ (similar to the expansion of the radius dependence of the spherical Green's function for small z).

For $\rho \to \infty$ the argument of the arctangent of Equation (8) approaches a constant, while $R_0 \to \rho$. Therefore, $\Phi'(\rho) \to \beta$, and $\Phi''(\rho) \to 0$, and thus $\delta(\rho) \to 0$. Equations (5) and (6) are solved in this limit to give:

$$\beta_z|_{\rho\to\infty} = 0$$
$$\alpha_z|_{\rho\to\infty} = \alpha$$

Armed with these physical arguments for limiting behavior, the approximation form of α_z and β_z are selected to be:

$$\alpha_z \approx \alpha \tag{11a}$$

$$\beta_z \approx \frac{\beta}{\sqrt{1 + (\frac{\rho}{B_1})^2 + (\frac{\rho}{B_2})^4 + (\frac{\rho}{B_3})^6}} \tag{11b}$$

with the coefficients B_1, B_2, and B_3 to be found by numerically solving the non-linear differential Equations (5) and (8). The assumption of Equation (11a) simplifies these equations considerably. This assumption is reasonable, since $\alpha_z(0) = \alpha$, $\alpha_z(\infty) = \alpha$, and all other radial variations in this problem are monotonic. Also, since the amplitude is specified to be uniform on the surface for all radii, it makes sense for the media loss to be solely and entirely dependent on the axial coordinate.

Equation (6) need not be solved to determine the ideal phase function. However, since $\Upsilon(\rho)$ is unconstrained, except for its value at $\rho = 0$, it can assume any functional dependence required to solve Equation (6).

To find the coefficients of Equation (11b), Equation (9) is squared and substituted into Equation (5), yielding:

$$1 - \frac{1}{1 + (\frac{\rho}{B_1})^2 + (\frac{\rho}{B_2})^4 + (\frac{\rho}{B_3})^6} \approx (\frac{\rho}{R_0} + \frac{\delta(\rho)}{\beta})^2 \tag{12}$$

which is solved for each ρ^{2n} term. Note that since the argument of the arctangent function of Equation (8) is a function of ρ^2, $\delta(\rho)$ is an odd function of ρ, and the right hand side of Equation (12) is an even function of ρ. The series form of β_z approximates the focusing phase derivative well, while maintaining the correct initial and final values. To solve exactly Equation (12) would require an infinite series of even powers of ρ in the approximation of β_z, but as long as the error between the left and right hand sides of Equation (12) is small—especially for small radii, where the source field most strongly affects the focused

field—only three terms are necessary. This is explicitly shown to be true in the numerical example in a following section.

Although the selection of a_z seems unsubstantiated, and Equation (6) is used only to establish limiting behavior, as long as the solution for the source phase distribution $\Phi(\rho')$ specifies electric field which is self-consistent with the Helmholtz Equation and also gives an entirely positive integrand in Equation (7), it represents the optimal solution. The computation leading to this result is approximate to the extent that the amplitude is assumed to vary no more rapidly than exponentially in the normal direction (which, in fact, is observed in the power pattern results section), and that the phase correction is approximated by a three-term series (with extremely small error).

Secondary Maximum Suppression

Solving for the phase in the preceding section yields the best uniform amplitude electric field source distribution for maximizing power at the center of the planar tissue slab. The thickest slab which can safely be heated would be that for which the focal power is the *same* as the surface power and higher than any secondary volume field maximum. Higher surface power than the focal power risks overheating tissue close to the sources; while lower focal than surface power would allow a thicker slab to be safely heated.

Using the source distribution derived in the preceding section at 915 MHz unfortunately generates a symmetric pair of secondary electric field maxima along the z axis. These maxima must be reduced to below the focal field value to avoid overheating healthy intervening tissue. By slightly adjusting the source distribution, it is possible to correct the pattern, lowering the secondary maxima fields, without significantly affecting the focal field.

These secondary maxima, each of which is closer to one source plane or the other than the focal maximum, are more sensitive to the surface source regions close to the z-axis. Introducing a minor constant phase shift for source points in the region $\rho < a$ will have a strong destructive effect on the secondary maximum, since the phase of each source contribution varies considerably with radius. However, the focal maximum will not change as much, because the entire in-phase source region $\rho < a$ is phase shifted by the same amount. Of course, the maximum slab thickness will have to be reduced slightly, since the focal field will no longer be the ideal integral of purely positive contributions. Instead, the field at the origin will be the vector sum of two phasors separated by a small angle θ. The vector sum must be unity, so the sum of the magnitudes of the vectors (which in the previous ideal case simply equaled the focal field) must be a slightly larger than one. The equation for determining θ is follows from the Law of Cosines,

$$\theta = \cos^{-1} \frac{I_1^2 + I_2^2 - 1}{2 I_1 I_2} \tag{13}$$

where

$$I_1 = \int_0^a \rho d\rho' \int_0^{2\pi} d\phi' \mathcal{I}$$

$$I_2 = \int_a^\infty \rho d\rho' \int_0^{2\pi} d\phi' \mathcal{I}$$

and $\mathcal{I}$ is the integrand of Equation (7).

The field throughout the volume is thus given by:

$$\bar{E}(\bar{r}) = I_1 e^{j\theta} + I_2 \tag{14}$$

with the same values of the functions α_z, β_z, and Φ as in Equation (7), and the source-to-observer distance $R = \sqrt{(d/2 \pm z)^2 + \rho'^2 + \rho^2 - 2\rho'\rho\cos(\phi' - \phi)}$.

It is not important what the "best" value of radius a might be, as long as the angle θ is small, and the secondary fields levels are lowered to below the focal and surface field levels.

Maximum Slab Thickness Determination

An iterative procedure is used to find the thickest HWC tissue slab model with a central global maximum at 915 MHz. First, an arbitrary slab thickness d is selected, say, one wavelength. The required focused phase distribution, $\Phi(\rho)$, is obtained as described above, and the power pattern is calculated using Equation (7) along with the values of β_z and α_z $(= \alpha)$ as stated in Equation (11). If the focal target power at $z = 0$ is greater than the surface or other secondary peak power, the slab thickness d is increased.

When the maximum thickness is reached, a radius a is selected for the constant phase shift to lower the secondary maxima of the power pattern. Once the greatest focal power peak is found, d is again increased, and the ideal focusing phase is recalculated.

The material characteristics of HWC tissue at 915 MHz are $\lambda = 4.46$ cm, $\beta = 1.40$ cm^{-1} and $\alpha = 0.322$ cm^{-1}. The result of the iteration gives a maximum thickness $d = 11.3$ cm. The best coefficients for the approximation of Equation (12) for $d = 11.3$ cm are: $B_1 = 5.615$, $B_2 = 13.74$, and $B_3 = 19.3$ cm. Note that several significant digits are necessary to accurately specify these coefficients since the phase correction function $\delta(\rho)$ is of order unity radians/cm, its approximation should be accurate to at least two places, and the series representing the approximation should be correct within two additional places. The series approximation error for $\delta(\rho')$ phase is shown in Figure 2. This phase *derivative* error is presented rather than phase error since the derivative is being approximated in Equation (12), and the numerical integration needed to obtain the phase may introduce further error. It is seen in Figure 2 that the worst error occurs at about 35 cm, or 8 wavelengths from the focal axis, with a value of one-half of one percent of a radian (0.3°)

per centimeter. Inside a two wavelength source radius, the error is less than 0.0003 radians per cm.—clearly acceptable within the scope of this biological problem, where the measured electrical parameters are accurate to at most 1 %.

The resulting focused phase is given in Figure 3, along with the simple conjugate phase function with zero offset. Figure 4 shows a detail of the correction to the phase as a function of radius. Mathematically, this is a plot of the arctangent function of Equation (8). The correction is greatest at the focal axis, lowering the conjugate phase value by almost 1.28 radians. It falls off with increasing radius to 0.92 radians at $\rho = 25$ cm or 5.5 wavelengths. This amounts to about 20° variation in a radius of 5.5 λ. This correction function does not vary much compared to the conjugate phase distribution; however, to determine the optimum power deposition pattern, all contributing factors must be considered. The difference between the electric field at the focal point resulting from the conjugate phase and from the ideal phase distributions amounts to about 0.1%, so the conjugate phase distribution is sufficient for focusing.

Power Pattern Results

Figure 5 shows three power patterns for electromagnetic radiation at 915 MHz in an infinitely wide slab of muscle tissue with thickness $d = 2.54\lambda = 11.3$ cm, as a function of distance from the focal target at the mid-plane. Each pattern is normalized to the power at the slab surface. The pattern with the least power at the focus $z = 0$ represents dissipated power for uniform phase and unity amplitude opposing sources located at $z = \pm\frac{d}{2}$. Its functional dependence is $P = |\cos(\beta - j\alpha)z|^2 / |\cos(\beta - j\alpha)\frac{d}{2}|^2$ [Rappaport, 1986]. For this slab thickness, all tissue more than 1.76 cm, or 0.4λ away from the mid-plane is overheated.

With phase focusing, including the lossy media correction function, the power at the focus increases by almost an order of magnitude. The slab thickness for which the surface power equals the focal power is $d = 11.4$cm. Slight overheating occurs at the secondary maximum near 3.0 cm out from the mid-plane. Of course, this secondary peak can be reduced with a thinner slab by placing the sources closer to the focal target.

Phase shifting the source within the region $\rho < a = 3$cm and using Equation (13) to find the shift $\theta = .40081$ changes the absolute power at the focus very slightly from the uniform amplitude case, while reducing the secondary peak to the level of the focal power. The limiting thickness, $d = 11.3$ is determined by this pattern. The sacrifice from introducing the constant phase shift decreases the maximum thickness 0.1 cm, less than 1%. The maximum thickness has increased over the uniform phase illumination by a factor of 3.2. Figure 5c represents the maximum amount of power delivered to the deepest point in a planar slab without risking overheating any other regions. Thus 5.65 cm is the deepest possible safe heating depth from plane microwave sources.

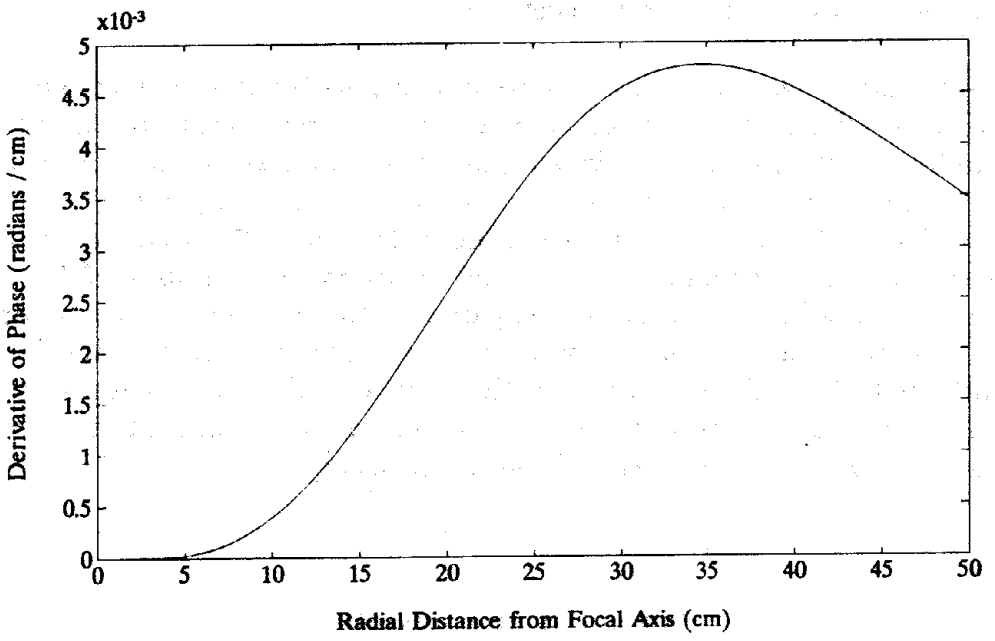

Figure 2: Error between the derivatives of focusing phase and the series approximation of $\sqrt{\beta^2 - \beta_z^2}$ for $d = 11.3$ cm.

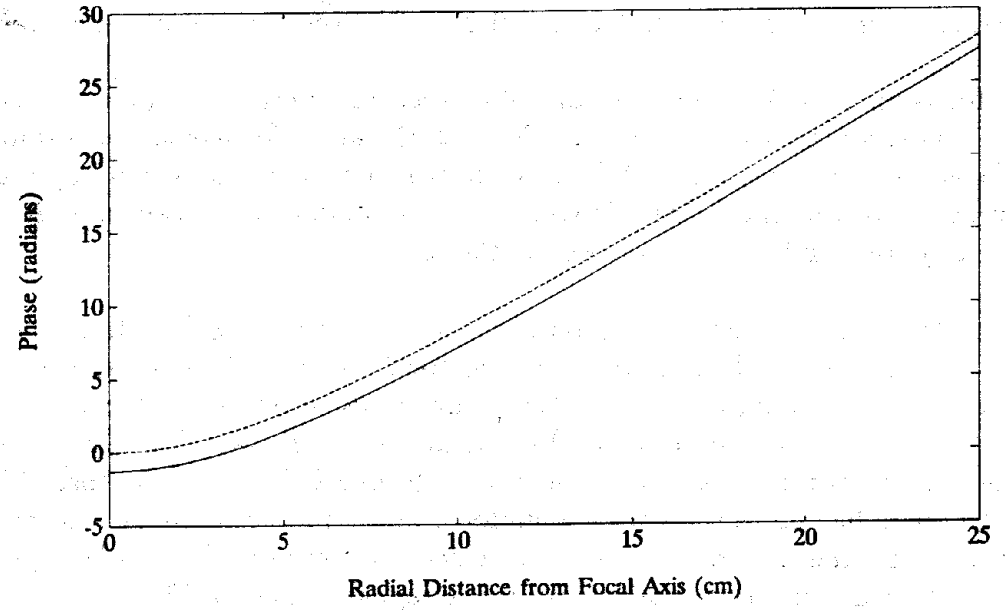

Figure 3: Conjugate (dashed) and ideal (solid) phase functions for focusing at a point on the mid-plane of a $d = 11.3$ cm thick slab of high water content biological tissue from the source plane at 915 MHz.

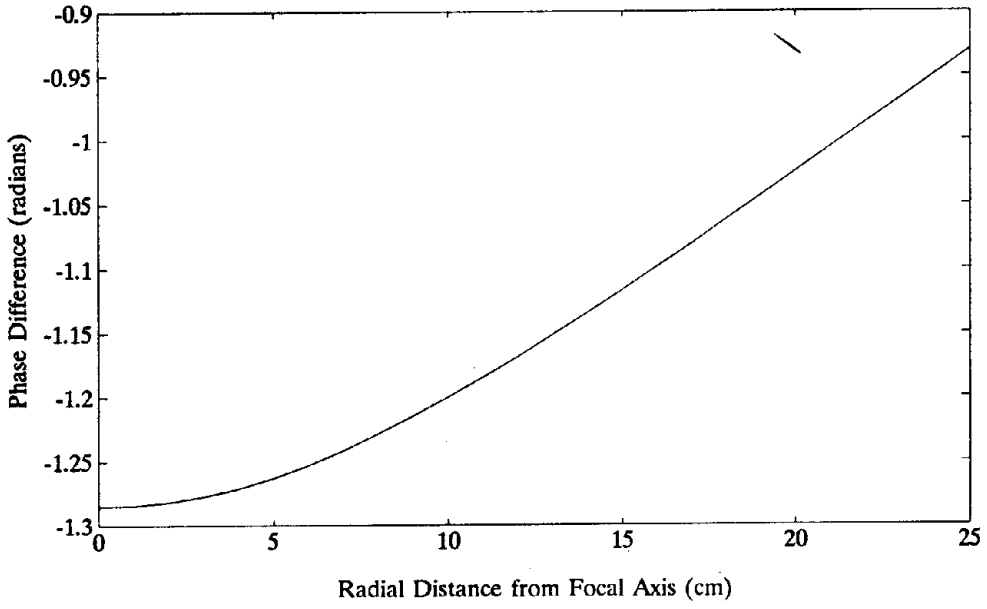

Figure 4: Correction function for complex integrand for focusing 915 MHz radiation at $d/2 = 5.65$ cm depth.

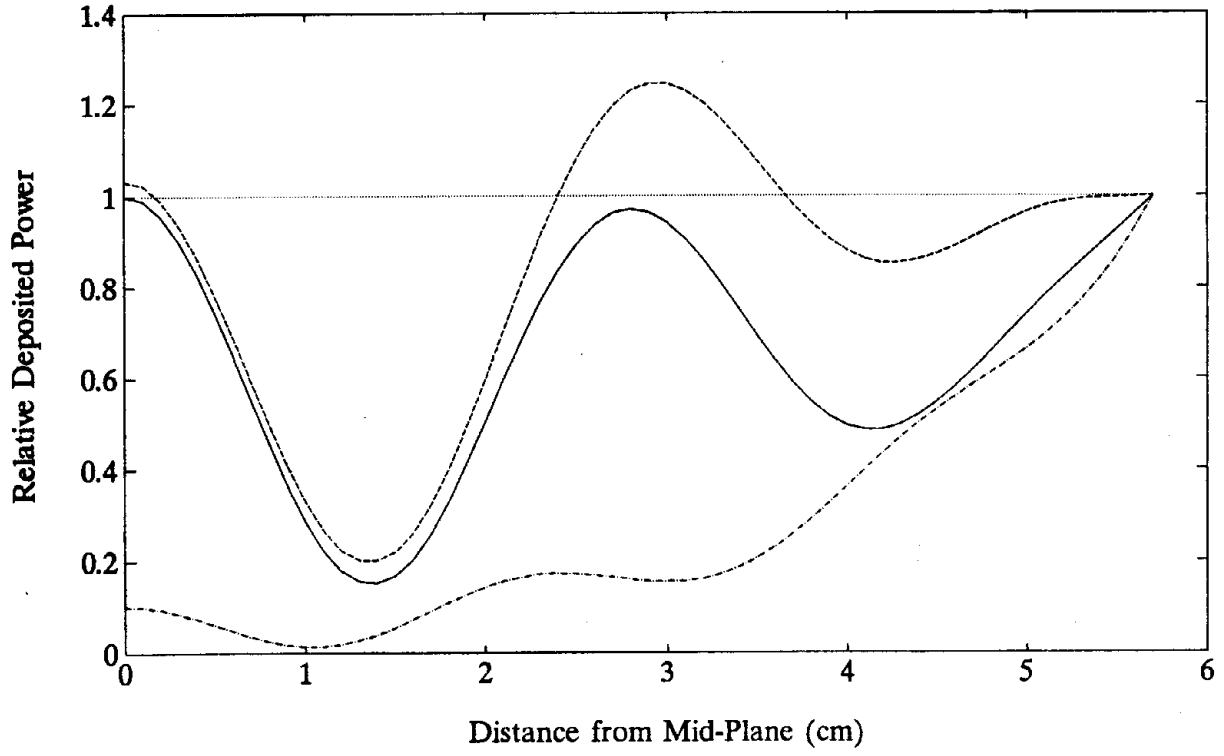

Figure 5: Power patterns for 915 MHz opposing planar sources: a) uniform source phase (dashed-dotted), b) phase focused unit amplitude (dashed), and c) phase focused with phase shift of .40081 for $\rho < 3$cm (solid).

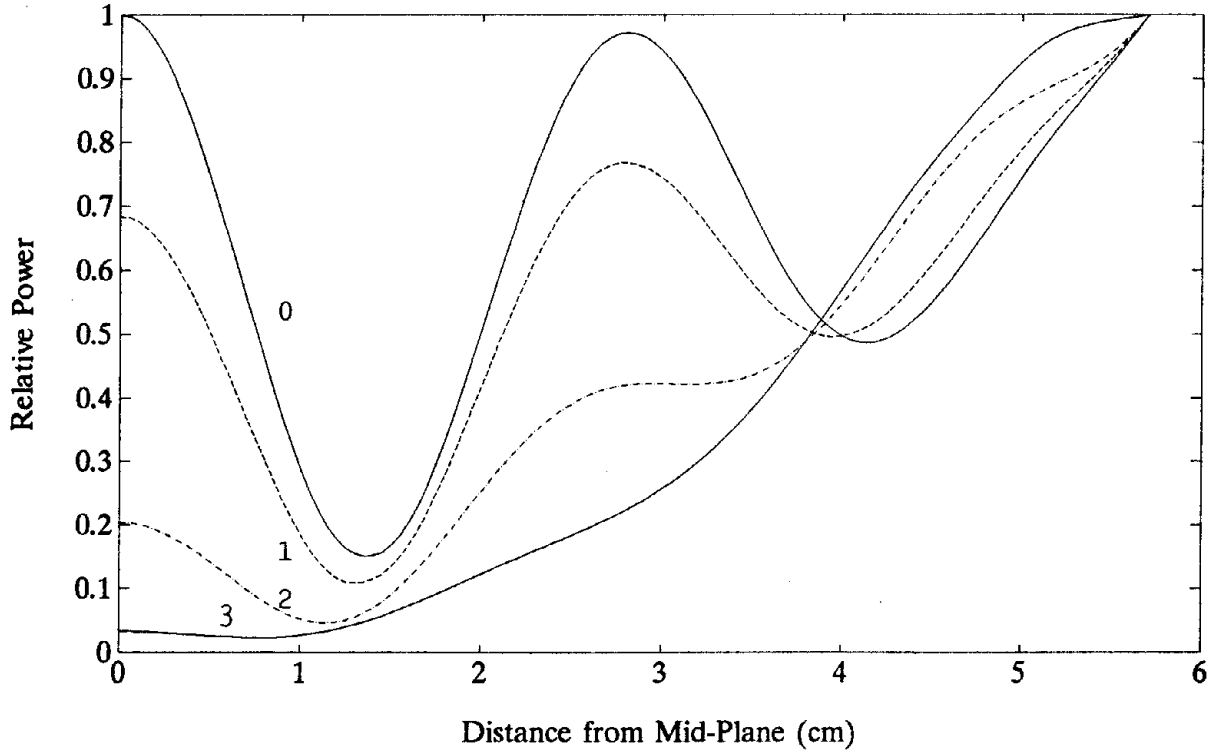

Figure 6: Optimum phase focused axial power deposition patterns for radial positions $\rho = 0,\ 1.0,\ 2.0$, and 3.0 cm.

As a check, the axial power patterns for four radial positions: $\rho = 0,\ 1.0,\ 2.0$, and 3.0 cm for the optimized source distribution of Figure 5c is shown in Figure 6. The focal power at $z = 0$ falls off to about two-thirds at $\rho = 1.0$ cm, and is almost negligible for greater radii.

Conclusions

The source excitation phase distribution for safely and efficiently heating the center of a planar slab of high water content tissue have been optimized. Corrections to the lossless conjugate phase focusing distribution produce only minimal increases in focal power.

The best planar source distribution can deposit a global power maximum in the center of a tissue volume more than three times thicker than for a uniformly excited slab. This power pattern is the best theoretical pattern. It may not be possible to duplicate the desired source phases and amplitudes with real hyperthermia applicators, but this pattern provides an ideal benchmark for determining feasibility of treatment.

It is conceivable that a different choice of constant phase shifting of part of the distribution might increase the ratio of focal point power to secondary maximum power without significantly suppressing the former below the surface power. However, this improvement is insignificant, especially in view of the large variation of measured tissue electrical characteristics.

References

1. Gee, W., Lee, S.W., Bong, N.K., Cain, C.A., Mittra, R., and Magin, R.L., "Focused Array Hyperthermia Applicator: Theory and Experiment," *IEEE Trans. Biomedical Engineering*, vol. BME-31, no. 1, January 1984, pp. 38-46.

2. Hahn, G., *Hyperthermia and Cancer*, New York: Plenum, 1982.

3. Johnson, C., and Guy, A., "Nonionizing electromagnetic wave effects in biological materials and systems," *Proc. IEEE*, vol. 60, pp. 692-718, June 1972.

4. Jouvie, F., Bolomey, J., and Gaboriaud, G., "Discussion of Capabilities of Microwave Phased Arrays for Hyperthermia Treatment of Neck Tumors", *IEEE Trans. Microwave Theory Tech.*, vol. MTT-34, no. 5, May 1986, pp. 495-501.

5. Kong, J., *Electromagnetic Wave Theory*, Wiley: New York, 1986.

6. Loane, J., Ling, H., Wang, B., and Lee, S., "Experimental Investigation of a Retro-Focusing Microwave Hyperthermia Applicator: Conjugate Field Matching Scheme," *IEEE Trans. Microwave Theory Tech.*, vol. MTT-34, no. 5, May 1986, pp. 490-493.

7. Overgaard, K., and Overgaard, J., "Investigations on the Possibility of a Thermic Tumor Therapy–I," *European Journal of Cancer*, vol. 8, no. 1, 1972, pp. 65-78.

8. Pereira, J. and Rappaport, C., "Optimal Microwave Source Distribution for Heating Off-Center Tumors in Biological Spheres," *1991 IEEE EMBS Symposium Digest*, vol. 2, October 1991, pp. 978-979.

9. Rappaport, C. and Morgenthaler, F., "Localized Hyperthermia with Electromagnetic Arrays and the Leaky Wave Troughguide Applicator," (Invited paper) *IEEE Trans. on Microwave Theory and Techniques*, May 1986, pp. 636-643.

10. Rappaport, C. and Morgenthaler, F., "Optimal Source Distribution for Hyperthermia at the Center of a Sphere of Muscle Tissue," *IEEE Trans. on Microwave Theory and Techniques*, December 1987, pp. 1322-1327.

11. Rappaport, C., *Synthesis of Optimum Microwave Antenna Applicators for Use in Treating Deep Localized Tumors*, in the *Progress in Electromagnetic Research* series, Ed. Jin Au Kong. New York: Elsevier, 1988.

12. Strohbehn, J., and Turner, P., "Physical Hyperthermia and Cancer Therapy," *IEEE Proceedings*, vol. 68, no. 1, January 1984, pp. 779-787.